the APD as a function of time at room ambient condition with an APD reverse bias of 123 V. The I-V characteristics before and after the reliability test are shown in Fig. 3. The initial current density is 118 A/cm^2. After the 25-hour test, the current density is ~119 A/cm^2 and the power density is 1.4×10^4 W/cm^2. The maximum and minimum current density during the 25-hour test are 117 and 121 A/cm^2, respectively. The fluctuation is < 3%. Note that the junction temperature of the APD can be expected to be much higher than room temperature due to the joule heating of 1.4×10^4 W/cm^2 although we cannot get a good measure of the junction temperature. After the reliability measurement, the reverse I-V characteristics were retested and compared with prior results. The major breakdown features, such as the breakdown voltage and the sharpness of the breakdown, are almost the same except for a higher leakage current, suggesting that MJTE terminated 4H-SiC APDs are very robust at room temperature and the stability is good. The increase in the leakage current is likely to be due to the non-impervious nature of the SiO_2, suggesting the need for Si_3N_4 passivation and sealing of the device.

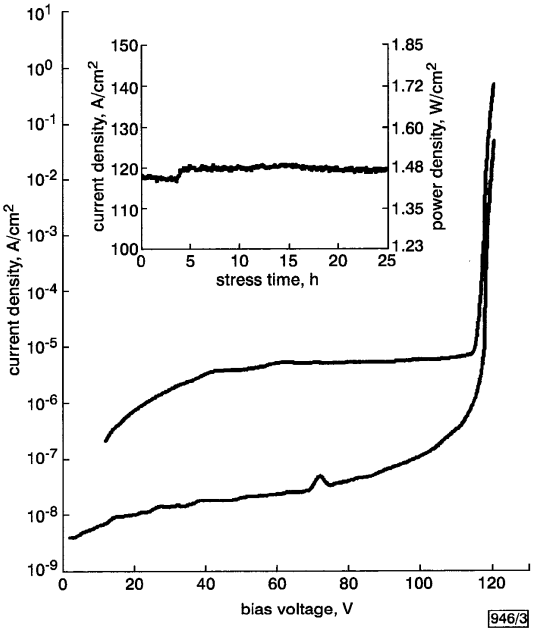

Fig. 3 *Reverse I-V characteristics before and after reliability test*
Inset: Reliability test of MJTE terminated 4H-SiC APDs

Conclusion: MJTE terminated 4H-SiC APDs have been fabricated. The leakage current at 95% of the breakdown level can be lower than 1 μA/cm^2 for devices with device area up to 300 × 300 μm^2. The peak responsivity is higher than 10^5 A/W. These APDs run very stably at room temperature with the power densities up to 1.4×10^4 W/cm^2.

Acknowledgment: The authors would like to acknowledge the financial support provided by a NASA SBIR programme, managed by V. Shields.

4 June 2001
Electronics Letters Online No: 20010720
DOI: 10.1049/el:20010720

F. Yan, Y. Luo, and J.H. Zhao (*SiCLAB, Department of ECE, Rutgers University, 94 Brett Road, Piscataway, NJ 08854, USA*)

E-mail: fengyan@ece.rutgers.edu

M. Bush and G.H. Olsen (*Sensors Unlimited, Inc., 3049 US Route 1, Princeton, NJ 08540, USA*)

M. Weiner (*United Silicon Carbide, Inc., 100 Jersey Ave., NJ 08901, USA*)

References

1 YAN, F., LUO, Y., ZHAO, J., and OLSEN, G.: '4H-SiC visible blind UV avalanche photodiode', *Electron. Lett.*, 1999, **35**, (11), pp. 929–930

2 CARRANO, J., LAMBERT, D., EITING, C., COLLINS, C., LI, T., WANG, S., YANG, B., BECK, A., DUPUIS, R., and CAMPELL, J.: 'GaN avalanche photodiodes', *Appl. Phys. Lett.*, 2000, **76**, (7), pp. 924–927

3 LI, X., TONE, K., FURSIN, L., ZHAO, J., BURKE, T., ALEXANDROV, P., PAN, M., and WEINER, M.: 'Multi-step junction termination extension for SiC power devices', *Electron. Lett.*, 2001, **37**, (6), pp. 392–393

4 KONSTANTINOV, A., NORDELL, N., WAHAB, Q., and LINDEFELT, U.: 'Temperature dependence of avalanche breakdown for epitaxial diodes in 4H-SiC', *Appl. Phys. Lett.*, 1998, **73**, (13), pp. 1850–1852

Low-noise single-photon detection at wavelength 1.55 μm

P.A. Hiskett, J.M. Smith, G.S. Buller and P.D. Townsend

The photon-counting performance of commercially available InGaAs/InP avalanche photodiodes operated in Geiger mode was investigated at temperatures between 77 and 260 K. In particular, their noise equivalent power was measured to be 4×10^{-17} WHz$^{-1/2}$ at 77 K. The implications of these results in the context of a quantum cryptography application are discussed.

Introduction: During the past few years there has been a steadily increasing interest in semiconductor-based photon counting detectors in the wavelength range 1.3–1.6 μm for the applications of time-resolved fluorescence [1, 2], optical time domain reflectometry [3] and quantum cryptography [4 – 6]. This Letter presents results on new InGaAs/InP-based avalanche photodiodes (APDs), model EPM 239AA manufactured by Epitaxx Ltd. (New Jersey, USA). These 40 μm-diameter, substrate entry devices were designed specifically for low leakage current at room temperature. We report on the operation of these diodes in Geiger mode, i.e. biased above avalanche breakdown voltage, in order to assess their performance as photon-counting detectors. While exhibiting detection efficiencies and temporal response comparable to other commercially available devices, the dark count rates were approximately 100 times less than the previously-reported best InGaAs/InP Geiger-mode photodiodes – thus opening up exciting possibilities in infrared photon-counting applications areas.

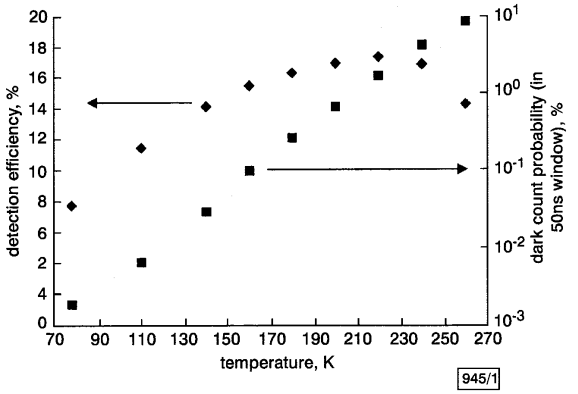

Fig. 1 *Detection efficiency and dark count probability (normalised to 50 ns window) against operating temperature*

Results: A current-voltage analysis of a specimen representative of the set of devices, revealed a multiplied dark current (at 97.5% of the breakdown voltage) of only 30 pA. By comparison, alternative commercially available InGaAs-based APDs were found to exhibit dark currents under these conditions of approximately 1–10 nA [7]. To characterise the APD in Geiger mode, the fibre-pigtailed detector was placed in a liquid nitrogen cryostat, and connected to a passively Q-switched (1550 nm) laser diode that produced pulses of 35 ps duration. This technique is more completely described in a recent paper by this group [7]. In summary, such an approach permits the almost simultaneous measurement of dark count rate, detection efficiency and temporal response at any set temperature between 77 and 260 K. The SPAD was operated in gated mode,

i.e. periodically held above breakdown for a short length of time, 162 ns in this case. The gating was controlled by an active quench circuit and synchronised to the optical pulses emitted from the laser. The results of the characterisation are shown in Fig. 1, which shows the detection efficiency and dark count probability at temperatures between 77 and 260 K for a bias of 3 V above the breakdown voltage. For these measurements, the repetition rate of the laser (and of the gate) was deliberately kept low (1 kHz) to minimise the effects of afterpulsing (see below). At 3 V excess bias, the temporal response varies between 270 ps (at 77 K) and 324 ps (at 260 K). Fig. 1 shows a typical behaviour for such a diode in that the dark count rate increases rapidly with temperature, as thermally generated carriers constitute the dominant contribution to the dark count probability. The dark count probability is only 1.8×10^{-5} in a 50 ns time window at 77 K, which is approximately 100 times less than the previously reported lowest value measured from a large sample of commercially available APDs cooled to 77 K at the same excess bias [7]. The detection efficiencies are comparable to these previous results.

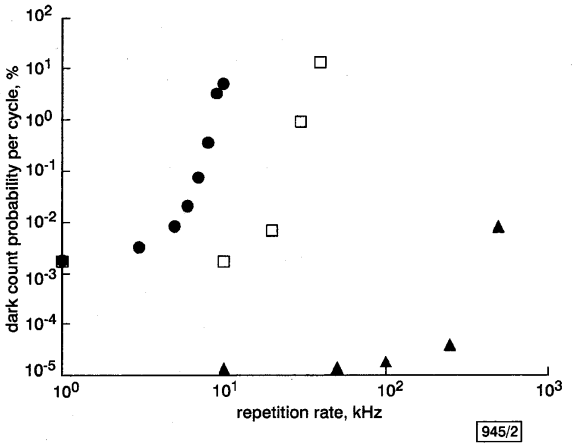

Fig. 2 *Graph of dark count probability per cycle against gate repetition rate for Epitaxx APD at 77 K at 3 V excess bias*

● active quench circuit (in 50 ns window)
□ passive quench circuit (in 50 ns window)
▲ gated mode (using 3.5 ns gate)

The problem of afterpulsing in cooled semiconductor-based photon-counting diodes has been noted by a number of authors [3, 8, 9]. The origin of this afterpulsing is likely to be the emission of carriers from trap states, which can lead to a spurious count if the carriers reach the multiplication region and trigger an avalanche. This problem is more evident at lower temperatures as the trap lifetimes lengthen and become comparable to the period between incident laser pulses. To assess the effects of afterpulsing in this low-noise detector, the repetition rate of the gate to the SPAD was varied, with no light incident on the detector. To more fully characterise the afterpulsing phenomenon, the gating rate dependence of the dark count probability was measured, for the same detector, in three different operating regimes: active quenching (described in [10, 11]); passive quenching (described in [12]); and short-gating mode (described in [9]). Some form of external quenching technique is necessary to stop the self-sustaining current pulse that occurs in a diode operated in Geiger mode after an avalanche is triggered (either by a photon or by a thermally generated carrier). Each operating technique has its advantages and disadvantages depending both on the diode performance parameters and end application. The detector was used at its optimum dark count rate condition at 77 K, and the repetition rate was varied to analyse its effect on the dark count probability. The speed of the quenching process in stopping the otherwise self-sustaining avalanche will directly affect the amount of charge flowing through the device, and thus the number of trap states filled per event. Hence the three operating techniques will result in different numbers of filled trap states, as clearly illustrated by the behaviour of the dark count probability against frequency, for an excess bias of 3 V, shown in Fig. 2. With the particular method of active quenching used (i.e. a remote Silena 8619 NIM module), the charge flow during the avalanche was great enough to fill a sufficient number of traps to observe an increased dark count rate at a frequency of only a few kHz. With passive quenching (using a 100 kΩ quenching resistor), the effect is only seen at frequencies of > 10 kHz. In both the active and passive quenching results, the detector was gated above breakdown for 162 ns after the laser pulse, however, the dark count probability from only a 50 ns window of this gate is shown. The short-gating mode technique relies on a short electrical pulse being placed across the diode to bias the device above breakdown for its duration. If an event occurs in this short time window, the end of the electrical pulse will bring the bias voltage below breakdown and effectively quench the avalanche. However, for such a technique to be more effective the pulse must be shorter than the charging time experienced in passive or active quenching. For the results shown in Fig. 2, the gate width was ~3.5 ns. Under these conditions the detector exhibited good performance up to several hundreds of kHz. The detector jitter (full-width-at-half-maximum) was measured to be around 270 ps, regardless of the quenching technique employed.

Discussion: To assess the potential of these detectors for infrared photon-counting applications, appropriate figures of merit can be calculated from the data given above. In terms of time-resolved fluorescence spectroscopy or optical time domain reflectometry one useful (but not comprehensive) figure of merit is noise equivalent power (NEP), which is defined as the signal power required to attain a unity signal-to-noise ratio within a 1 s integration time [3]. The NEP is given by [3]

$$NEP = \frac{h\nu}{DE}\sqrt{2N_D}$$

where DE is the detection efficiency, N_D is the normalised dark count rate, ν the frequency of light used and h is Planck's constant. The minimum NEP for the Epitaxx APD results then in 4×10^{-17} WHz$^{-1/2}$, compared with a value of 4×10^{-16} WHz$^{-1/2}$ measured for the best Fujitsu InGaAs/InP APD (model FPD13U81SR) at the same operating temperature [7].

However, the optimum operating condition for a SPAD is not simply at the temperature where the NEP is at a minimum because of the effects of afterpulsing. These results were obtained at 1 kHz and, therefore, afterpulsing was minimal. At this very low frequency the optimum operating temperature would indeed be 77 K. Nonetheless, if the application demanded a higher operating frequency, a common case in quantum cryptography, then the temperature of 77 K would not be a suitable choice because of the long trap lifetimes at this temperature. A higher temperature would be necessary to reduce the effects of afterpulsing even at the expense of higher thermally induced dark counts.

Conclusions: A new low-noise InGaAs APD has been operated in photon-counting mode at temperatures between 77 and 260 K. The results indicate a reduction in dark count probability of a factor of ~100 and an improvement in NEP of a factor of 10 over other InGaAs diodes at a wavelength of 1.55 μm. The effect of different quenching techniques has been investigated and, when used in gated mode with a sufficiently short gate duration, repetition rates of hundreds of kHz were achieved with no significant afterpulsing effects.

Recent results [13] show that incorporating this detector, operated at 140 K, into a quantum cryptography receiver operating at 100 kHz allowed transmission distance of 80 km to be realised. The measured quantum bit error rate of this 80 km system was measured to be 9%. This is considerably beyond the 40–50 km range that has been reported to date [4, 5].

4 June 2001
Electronics Letters Online No: 20010734
DOI: 10.1049/el:20010734

P.A. Hiskett, J.M. Smith and G.S. Buller (*Department of Physics, Heriot-Watt University, Riccarton, Edinburgh EH14 4AS, United Kingdom*)

P.D. Townsend (*Corning Research Centre, Adastral Park, Martlesham Heath, Ipswich, IP5 3RE, United Kingdom*)

References

1 BULLER, G.S., FANCEY, S.J., MASSA, J.S., WALKER, A.C., COVA, S., and LACAITA, L.: 'Time-resolved photoluminescence measurements of InGaAs/InP multiple-quantum-well structures at 1.3 micron wavelengths by use of germanium single-photon avalanche photodiodes', *Appl. Opt.*, 1996, **35**, (6), pp. 916–921

2 FANCEY, S.J., BULLER, G.S., MASSA, J.S., WALKER, A.C., MCLEAN, C.J., MCKEE, A., BRYCE, A.C., MARSH, J.H., and DE LA RUE, R.M.: 'Time-resolved photoluminescence microscopy of GaInAs/GaInAsP multiple quantum wells intermixed using a pulsed laser technique', *J. Appl. Phys.*, 1996, **79**, pp. 9390–9392

3 ZAPPA, F., LACAITA, A.L., COVA, S., and LOVATI, P.: 'Solid state single-photon detectors', *Opt. Eng.*, 1996, **35**, (4), pp. 938–945

4 TOWNSEND, P.D.: 'Quantum cryptography on optical fibre networks', *Opt. Fibre Technol.*, 1998, **4**, pp. 345–370

5 HUGHES, R.J., MORGAN, G.L., and PETERSON, C.G.: 'Quantum key distribution over a 48 km optical fibre network', *J. Mod. Opt.*, 2000, **47**, (2–3), pp. 533–547

6 RIBORDY, G., GAUTIER, J., GISIN, N., GUINNARD, O., and ZBINDEN, H.: 'Automated "plug and play" quantum key distribution', *Electron. Lett.*, 1998, **34**, (22), pp. 2116–2117

7 HISKETT, P.A., BULLER, G.S., LOUDON, A.Y., SMITH, J.M., GONTIJO, I., WALKER, A.C., TOWNSEND, P.D., and ROBERTSON, M.: 'Performance and design of InGaAs/InP photodiodes for single-photon counting at 1.55 μm', *Appl. Opt.*, 2000, **39**, (36)

8 LACAITA, A., ZAPPA, F., COVA, S., and LOVATI, P.: 'Single-photon detection beyond 1 micron: performance of commercially available InGaAs/InP detectors', *Appl. Opt.*, 1996, **35**, (16), pp. 2986–2996

9 RIBORDY, G., GAUTIER, J.D., ZBINDEN, H., and GISIN, N.: 'Performance of InGaAs/InP avalanche photodiodes as gated-mode photon counters', *Appl. Opt.*, 1998, **37**, (12), pp. 2272–2277

10 LACAITA, A., FRANCESE, P.A., ZAPPA, F., and COVA, S.: 'Single-photon detection beyond 1 micron: performance of commercially available germanium photodiodes', *Appl. Opt.*, 1994, **33**, (30), pp. 6902–6918

11 COVA, S., GHIONI, M., LACAITA, A., SAMORI, C., and ZAPPA, F.: 'Avalanche photodiodes and quenching circuits for single-photon detection', *Appl. Opt.*, 1996, **35**, (12), pp. 1956–1976

12 BROWN, R.G.W., RIDLEY, K.D., and RARITY, J.G.: 'Characterisation of silicon avalanche photodiodes for photon correlation measurements. 1: Passive quenching', *Appl. Opt.*, 1986, **25**, (22), pp. 4122–4126

13 HISKETT, P.A., BONFRATE, G., BULLER, G.S., and TOWNSEND, P.D.: '80 km transmission experiment using an InGaAs/InP SPAD-based quantum cryptography receiver operating at 1.55 μm', accepted for publication in *J. Mod. Opt.*

Correction of residual motion errors in airborne SAR interferometry

A. Reigber

The main limitation for a wider applicability of airborne repeat-pass interferometric SAR data is the presence of small uncompensated motion errors. The effect of residual motion compensation errors is addressed and a new technique to minimise their influence on the interferometric phase is proposed.

Introduction: One main problem in the interferometric processing of airborne repeat-pass SAR data is the presence of residual phase errors in the generated interferogram. Even though the effects of the turbulent aircraft motion can be compensated almost perfectly by a high-quality motion compensation during SAR processing [1], always small errors occur owing to inaccuracies in the exact estimation of the antenna position during the flight.

Very similar to the problem of atmospheric effects in spaceborne SAR interferograms, also the residual motion error has a differential effect. Therefore subcentimetre precision in the positioning would be required to obtain unaffected interferograms. This can hardly be reached at present. In the derived interferograms, the occurred residual motion errors appear usually as low-frequent phase modulations in azimuth. Therefore, for applications which require large-scale or multiple-image phase relations, e.g. differential interferometry or DEM generation, airborne repeat-pass data cannot be used. In the following, a technique is proposed which estimates the total residual motion error over both tracks out of the interferogram itself.

Algorithm description: Uncorrected motion errors affect SAR images mainly in two ways. First, the motion errors cause a distortion of the image phase. Each of the two images is affected by a phase error of

$$\Delta\Phi_{err}(x,r) = \frac{4\pi}{\lambda}\Delta r(x,r) \qquad (1)$$

with x and r denoting the azimuth and range position, respectively, λ the radar wavelength and Δr the uncompensated displacement from the real track in line-of-sight direction. The differential error between the two tracks can be observed directly in the interferometric phase. It appears usually as a phase modulation along azimuth with only a slight range dependency due to the change of the look angle from near-range to far-range.

Secondly, the residual motion errors cause spatial distortions in the processed image. A residual motion error modifies the ideal parabolic phase history of a target. If for example the error has a linear characteristic, i.e. if the real track is rotated by an angle α with respect to the measured one, the phase history of a target located in the range distance r_0 and at the azimuth position x_0 can be written as

$$\Phi(x) = \frac{4\pi}{\lambda}\left(r_0 + \frac{(x-x_0)^2}{2r_0} + 2x\sin\alpha\right) \qquad (2)$$

If the images are processed with zero Doppler-centroid, the maximum of the impulse response is focused at the place where the received azimuth signal passes frequency zero, i.e. where the deviation of its phase history becomes zero:

$$\frac{\partial}{\partial x}\Phi(x) = \frac{4\pi}{\lambda}\left(\frac{x-x_0}{r_0} + 2\sin\alpha\right) = 0$$
$$\Rightarrow \quad x = x_0 - 2r_0\sin\alpha \qquad (3)$$

Therefore, in case of a linear error, the peak appears shifted in azimuth by $\Delta x = 2r_0\sin\alpha$, i.e. by the deviation of the original phase error scaled with the range distance of the target. As uncorrected errors are usually only of the order of a few centimetres, this effect is relatively small and might not be very disturbing for the amplitude images.

During the coregistration of airborne SAR images, the spatially varying azimuth offset $\Delta x(x, r)$ has to be measured and corrected, in order to generate interferograms with high coherence. As mentioned above, this offset is proportional to the deviation of the differential residual error in both tracks. This differential error is again proportional to the observed phase error in the interferogram. Therefore, it can be estimated by integrating the observed azimuth offsets in azimuth direction:

$$\Delta\Phi_{err}(x,r) = \int \frac{2\pi\Delta x(x)}{\lambda r}dx + C_{absolute} \qquad (4)$$

The integration constant $C_{absolute}$ is unknown and cannot be resolved with this method. It causes only a global phase offset. To avoid sudden phase variations from one azimuth line to another, it has to be adjusted in a way that the variations of the derived error phase term are minimised over range. This leads to a smooth two-dimensional correction function.

The limitation of this method is the precision of the used coregistration method and its spatial resolution. Interferometric coregistration based on spectral diversity [2] reaches an accuracy of up to 1/100 of resolution element combined with high spatial resolution. Therefore, this method seems to be well suited to support the residual phase correction as proposed above.

Experimental results: The performance of the residual phase compensation was evaluated using airborne data acquired by the E-SAR in L-band repeat-pass mode in May 1998. The observed terrain of Oberpfaffenhofen/Germany has only slight topography. As, in addition, the baseline between the two paths was very small (< 10 m), the resulting interferogram should show nearly no phase variations. Looking at the interferogram, shown in Fig. 1, phase variation in azimuth of more than 400° can be observed. This indicates that the motion compensation of the nonlinear flight track was carried out only insufficiently. In this case the main reason was a technical problem with the navigation system, which did not record the position data with the usual precision.

In Fig. 2 the interferogram corrected by the phase term derived from the coregistration parameters is shown. As expected from the